

Model investigations of the correlation between the mean transverse momentum and anisotropic flow in shape-engineered events

Niseem Magdy^{1,*} and Roy A. Lacey²

¹*Department of Physics, University of Illinois at Chicago, Chicago, Illinois 60607, USA*

²*Department of Chemistry, State University of New York, Stony Brook, New York 11794, USA*

The correlation between the event mean-transverse momentum, $[p_T]$, and the anisotropic flow magnitude, v_n , $\rho(v_n^2, [p_T])$, has been argued to be sensitive to the initial conditions in heavy-ion collisions. We use simulated events generated with the AMPT and EPOS models, to investigate the model dependence, and the response and sensitivity of the $\rho(v_n^2, [p_T])$ correlator to collision-system size and shape, and the viscosity of the matter produced in the collisions. We find good qualitative agreement between the correlators for the string melting version of the AMPT model and the EPOS model. Detailed tests indicate that $\rho(v_n^2, [p_T])$ is sensitive to the initial-state geometry of the collision system, but is insensitive to sizable changes in the viscosity of the medium produced in the collisions. These findings suggest that precise differential measurements of $\rho(v_n^2, [p_T])$ as a function of system-size, shape and beam-energy could provide more stringent constraints to discern between initial-state models and hence, more reliable extractions of η/s .

Keywords: Collectivity, correlation, shear viscosity, transverse momentum correlations

I. INTRODUCTION

A central objective of the current heavy-ion programs at the Large Hadron Collider (LHC) and the Relativistic Heavy-Ion Collider (RHIC) is to understand the properties of the quark-gluon plasma (QGP) [1–3] formed in high-energy heavy-ion collisions. Substantial attention has been given to understand the QGP transport properties, particularly the ratio of shear viscosity η , to the entropy density s known as the specific shear viscosity (η/s). The specific shear viscosity (η/s) which encodes the ability of the QGP to transport momentum, has been extensively studied both theoretically and experimentally [4–7].

Observables that characterize the azimuthal anisotropy of particles emitted in the transverse plane, are among the key measurements that have been used to constrain the viscous hydrodynamic response to the initial spatial distribution in energy density, produced in the early stages of the collision [5, 8–22].

Many of the data-model comparisons at RHIC and the LHC have inferred a small η/s value for the QGP, albeit with sizable uncertainties [4–7, 16, 23]. The current consensus is that a major uncertainty in the η/s extractions, stem from the uncertainty in the estimates for the initial-state eccentricities employed in the model calculations. Thus, a wealth of ongoing theoretical and experimental studies have sought to identify observables that can give more detailed insight as well as new constraints for the initial-state geometry. A recent proposal is that the correlation coefficient $\rho(v_n^2, [p_T])$ [24–30];

$$\rho(v_n^2, [p_T]) = \frac{\text{cov}(v_n^2, [p_T])}{\sqrt{\text{Var}(v_n^2)}\sqrt{\text{Var}([p_T])}}, \quad (1)$$

might be more sensitive to the initial-state geometry, because it leverages the correlation between the eccentricity-driven flow harmonics v_n and the average transverse momentum of particles in an event $[p_T]$. The latter is related to the transverse size of the overlap region, so events that have similar energy-density but smaller initial-state transverse size should have a larger radial expansion and consequently larger mean transverse momentum [31]. It has also been proposed that the $\rho(v_n^2, [p_T])$ correlator is sensitive to the correlations between the initial size and the initial-state deformation of colliding nuclei [30, 32, 33]. Further detailed studies of the $\rho(v_n^2, [p_T])$ correlator are required to optimize its utility to discern between different initial-state models.

In this work, we use detailed simulations with both the AMPT [34], and EPOS [35–37] models, to study the $\rho(v_n^2, [p_T])$ correlators model dependence and its response and sensitivity to the magnitude of η/s and initial-state geometry.

The paper is organized as follows. Section II describes the theoretical models (AMPT and EPOS) and the analysis method employed to compute $\rho(v_n^2, [p_T])$. Sec. III, reports the results from our analysis, and is followed by a summary presented in Sec. IV.

II. METHODOLOGY

A. Models

This study is performed with simulated events for Au+Au collisions at $\sqrt{s_{NN}} = 200$ GeV, obtained with the AMPT [34], and EPOS [35–37] models. Computations were performed for charged hadrons in the transverse momentum range $0.2 < p_T < 2.0$ GeV/ c and the pseudorapidity acceptance $|\eta| < 1.0$. The latter choice mimics the acceptance of the STAR experiment at RHIC.

* niseemm@gmail.com

- **AMPT Model:** The AMPT model (version 2.26t9b) [34] has been widely used to study relativistic heavy-ion collisions at LHC and RHIC energies [34, 38–44]. In the current study, simulations were made with the string melting option both on and off. In such a situation when the string melting mechanism is on, hadrons created from the HIJING model are converted to their valence quarks and anti-quarks, and their evolution in time and space is then shaped by the ZPC parton cascade model [45]. The key elements of AMPT include (i) HIJING model [46, 47] initial parton-production stage, (ii) a parton scattering stage, (iii) hadronization through coalescence followed by (iv) a hadronic interaction stage [48]. In stage (ii) the used parton scattering cross-sections are evaluated according to;

$$\sigma_{pp} = \frac{9\pi\alpha_s^2}{2\mu^2}, \quad (2)$$

where α_s is the QCD coupling constant and μ is the screening mass in the partonic matter. They principally establish the expansion dynamics of the A+A collision systems [45]; Within the AMPT model framework, the η/s value can be adjusted via an appropriate choice of μ and/or α_s for a particular initial temperature T_i [49].

$$\frac{\eta}{s} = \frac{3\pi}{40\alpha_s^2} \frac{1}{\left(9 + \frac{\mu^2}{T^2}\right) \ln\left(\frac{18 + \mu^2/T^2}{\mu^2/T^2}\right) - 18}, \quad (3)$$

In the current work, Au+Au collisions at $\sqrt{s_{\text{NN}}} = 200$ GeV, were simulated with model version ampt-v2.26t9b for a fixed value $\alpha_s = 0.47$, but the shear viscosity η/s is varied over the range 0.1–0.3 by adjusting μ from $2.26 - 4.2 \text{ fm}^{-1}$ for a temperature $T_i = 378$ MeV [49]. The three AMPT sets which will be presented in this work are summarized in Tab. I.

AMPT-set	η/s	String Melting Mechanism
Set-1	0.1	OFF
Set-2	0.1	ON
Set-3	0.3	ON

TABLE I. The summary of the three AMPT sets which will be presented in this work.

- **EPOS Model:** The EPOS model [35–37] is based on a 3+1D viscous hydrodynamical description of A+A collisions. The initial state conditions are defined in terms of flux tubes estimated via Gribov-Regge multiple scattering theory [35]. EPOS can be subdivided into three main components, (i) the

core-corona division, (ii) the hydrodynamical evolution, and (iii) the hadronic cascades.

(i) The separation of the flux tubes fragmentation into *core* and *corona* (hadronize as a hadron jet) is based on the probability to escape from the bulk matter which will depend on the fragment transverse momentum and the local string density.

(ii) The hydrodynamical evolution based on the *vH-LLE*, viscous HLLC-based algorithm, 3D+1 viscous hydrodynamics employ a realistic Equation of State constrained with Lattice QCD data [50].

(iii) The hadronic cascade, *hadronic afterburner*, is based on the UrQMD model [51, 52], which has been broadly employed to investigate ultra-relativistic heavy-ion collisions [51–53]. UrQMD was designed to investigate hadron-hadron, hadron-nucleus, and heavy-ion collisions from $E_{\text{Lab}} = 100 \text{ A}\cdot\text{MeV}$ to $\sqrt{s_{\text{NN}}} = 200$ GeV. Therefore, it includes a collision term that accounts for the interactions of more than 50 (40) baryon (meson) species as well as their anti-particles. The UrQMD model describes the hadron-hadron interactions as well as the system evolution based on covariant propagation of all hadrons in the model with resonance decay, stochastic binary scattering, and color string formation.

The results reported in sec. II B, were obtained for minimum bias Au+Au collisions at $\sqrt{s_{\text{NN}}} = 200$ GeV. A total of approximately 4.0, 5.0, 3.0, and 0.3 M events of Au+Au collisions were generated with AMPT Set-1, Set-2, Set-3, and EPOS, respectively.

B. Analysis Method

The $\rho(v_n^2, [p_T])$ correlator is derived from covariances and variances (cf. Eq. 1) which involve both two- and multi-particle correlations that could also be influenced by non-flow effects due to resonance decays, Bose-Einstein correlations, and the fragments of individual jets [54]. Since non-flow contributions mostly involve particles emitted within a localized region in pseudorapidity, η , they can be mitigated via the sub-event cumulant methods [43, 55–57]. A major mitigating feature of these methods, is the correlation of particles from two or more sub-events which are separated in η . The efficacy of these methods to reduce non-flow effects have been quantified for many different two- and multi-particle correlators [55, 56].

In the current work, the two-subevent method is used to construct the v_2^2 variance. Thus, we use two separate η selections specified as $-1.0 < \eta_A < -0.35$ and $0.35 < \eta_C < 1.0$ to determine the v_2^2 variance as:

$$\begin{aligned} \text{Var}(v_2^2) &= v_2\{2\}^4 - v_2\{4\}^4, \\ &= C_2^2\{2\} - C_2\{4\}, \end{aligned} \quad (4)$$

where $v_2\{2\}$ and $v_2\{4\}$ are the flow coefficients obtained from the two- and four-particle correlations respectively, with the sub-event method [55] with particles in the region η_A and η_C ;

$$C_2\{2\} = \langle\langle 2 \rangle\rangle|_{A,C} = \langle\langle e^{i 2(\varphi_1^A - \varphi_2^C)} \rangle\rangle, \quad (5)$$

$$v_2\{2\} = \sqrt{C_2\{2\}} \quad (6)$$

where $\phi_{A(C)}$ is the azimuthal angle of particles in the region $A (C)$.

$$C_2\{4\} = \langle\langle 4 \rangle\rangle|_{A,C} - 2\langle\langle 2 \rangle\rangle^2|_{A,C}, \quad (7)$$

$$v_2\{4\} = \sqrt{C_2\{4\}} \quad (8)$$

where,

$$\langle\langle 4 \rangle\rangle|_{A,C} = \langle\langle e^{i 2(\varphi_1^A + \varphi_2^A - \varphi_3^C - \varphi_4^C)} \rangle\rangle. \quad (9)$$

The variance of the dynamical p_T fluctuations [58], $c_k \sim \text{Var}([p_T])$, defined in region $|\eta_B| < 0.35$, can be given as:

$$c_k = \left\langle \frac{1}{N_{\text{pair}}} \sum_B \sum_{B' \neq B} (p_{T,B} - \langle [p_T] \rangle) (p_{T,B'} - \langle [p_T] \rangle) \right\rangle, \quad (10)$$

where $\langle \rangle$ is an average over all events. The event mean p_T , $[p_T]$, is given as,

$$[p_T] = \sum_{i=1}^{M_B} p_{T,i} / M_B, \quad (11)$$

where M_B is the event multiplicity in sub-event B . The covariance between v_2^2 and $[p_T]$, $\text{cov}(v_2^2, [p_T])$, is defined using the three-subevents method [59, 60] as,

$$\text{cov}(v_2^2, [p_T]) = \text{Re} \left(\left\langle \sum_{A,C} e^{i2(\phi_A - \phi_C)} ([p_T] - \langle [p_T] \rangle)_B \right\rangle \right). \quad (12)$$

The resulting $\rho(v_2^2, [p_T])$ correlator, obtained via Eqs. 4, 10 and 12;

$$\rho(v_2^2, [p_T]) = \frac{\text{cov}(v_2^2, [p_T])}{\sqrt{\text{Var}(v_2^2)} \sqrt{c_k}}, \quad (13)$$

is similar to that used in prior studies [24–30].

III. RESULTS AND DISCUSSION

The $\rho(v_n^2, [p_T])$ correlator is derived from the correlations and fluctuations of v_n and p_T . Therefore, it is instructive to investigate the dependence of these variables on the models and the corresponding parameters tabulated in Table I. Fig. 1 shows a comparison of the centrality dependence of $v_2\{2\}$ (a), $v_2\{4\}$ (b) the ratios $v_2\{4\}/v_2\{2\}$ (c), and $\langle p_T \rangle$ (d) for the AMPT and EPOS

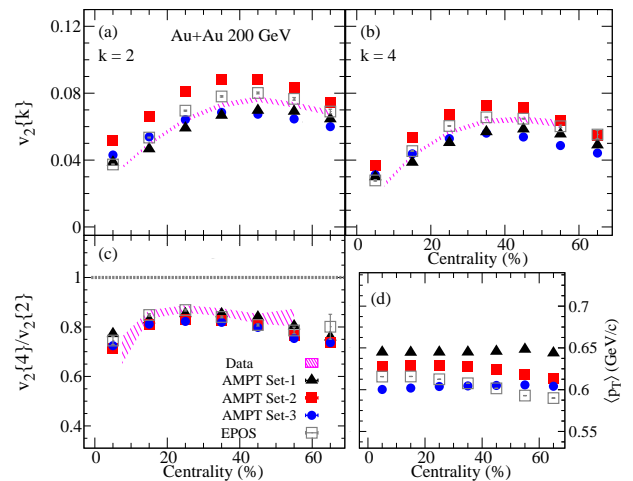


FIG. 1. Centrality dependence of $v_2\{2\}$ (a), $v_2\{4\}$ (b), $v_2\{4\}/v_2\{2\}$ (c) and $\langle p_T \rangle$ computed with the AMPT and EPOS models for Au+Au collisions at 200 GeV. The hatched bands represent the experimental data reported by the STAR collaboration [61].

models. Panels (a) and (b) indicate that the AMPT results are sensitive to both the viscosity and whether or not string melting is turned on. They also indicate similar qualitative patterns between both models and the data reported by the STAR collaboration [61] (hatched bands) over the range of the model parameters summarized in Table I.

The ratios $v_2\{4\}/v_2\{2\}$, shown in panel (c), serve as a figure of merit for the strength of the elliptic flow fluctuations; $v_2\{4\}/v_2\{2\} = r$ correspond to minimal flow fluctuations for $r \sim 1.0$ and sizable flow fluctuations for decreasing values of $r < 1$. The computed ratios, which are similar to the experimental ones, are to within $\sim 5\%$ insensitive to the model choice and the parameter sets tabulated in Tab. I, suggesting that the flow fluctuations are eccentricity-driven and are roughly a constant fraction of $v_2\{2\}$. The $\langle p_T \rangle$ values shown in panel (d) further indicate minor sensitivity to the models and the associated model parameters.

Figure 2 compare the centrality dependence of the values for $\text{Var}(v_2^2)$ (a), $\text{Var}([p_T])$ or c_k (b), $\text{cov}(v_2^2, [p_T])$ (c) and $\rho(v_2^2, [p_T])$ (d), computed for tracks with $0.2 < p_T < 2.0$ GeV/c in Au+Au collisions simulated with the AMPT and EPOS models. The comparisons show good overall agreement between the results for EPOS and those for AMPT with parameter Set-2. By contrast, panels (a) - (d) indicate sizable differences between the AMPT results for parameter Set-1 [string melting off] and Set-2 [string melting on]. These differences suggest that data-model comparisons of $\text{Var}(v_n^2)_{\text{dyn}}$, c_k , $\text{cov}(v_n^2, [p_T])$ and $\rho(v_n^2, [p_T])$ could serve as an important constraint for charting the respective roles of the partonic and hadronic phases in these collisions.

Figure 3 shows the influence of η/s on the values for $\text{Var}(v_2^2)$ (a), c_k (b), $\text{cov}(v_2^2, [p_T])$ (c) and $\rho(v_2^2, [p_T])$ (d).

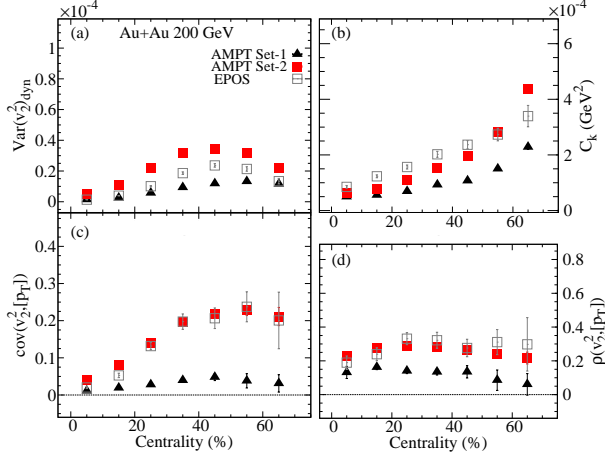


FIG. 2. Comparison of the centrality dependence of $\text{Var}(v_n^2)_{dyn}$ (a), c_k (b), $\text{cov}(v_n^2, [p_T])$ (c) and $\rho(v_n^2, [p_T])$ (d) obtained from the AMPT and EPOS models for Au+Au collisions at 200 GeV.

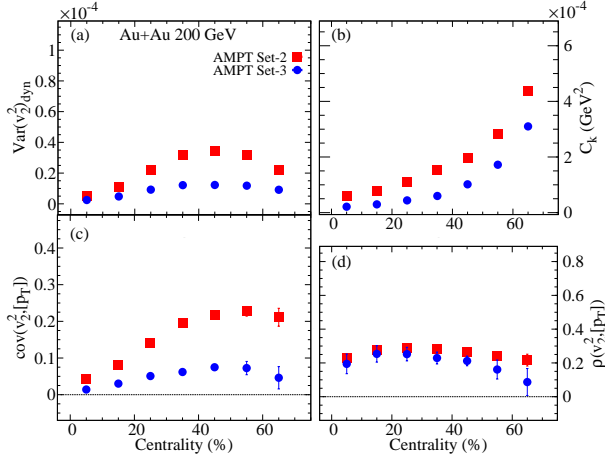


FIG. 3. Comparison of the centrality dependence of the values for $\text{Var}(v_n^2)_{dyn}$ (a), c_k (b), $\text{cov}(v_n^2, [p_T])$ (c) and $\rho(v_n^2, [p_T])$ (d), computed for Au+Au collisions at 200 GeV with the AMPT model. Results are compared for model parameter Set-2 ($\eta/s = 0.1$) and Set-3 ($\eta/s = 0.3$) as indicated.

Here, results from the AMPT model are shown for model parameter Set-2 ($\eta/s = 0.1$) and Set-3 ($\eta/s = 0.3$) as indicated. Figs. 3 (a) - (c) show that an increase in the magnitude of η/s reduces the values for $\text{Var}(v_n^2)$, c_k , and $\text{cov}(v_n^2, [p_T])$ for all centrality selections. By contrast, the $\rho(v_n^2, [p_T])$ values show little, if any, change, suggesting that an apparent cancellation of the effects of viscous attenuation renders the $\rho(v_n^2, [p_T])$ correlator insensitive to η/s .

Differential flow measurements $v_n(p_T)$ indicate that v_n is strongly correlated with p_T . Consequently, it is instructive to investigate the influence of a p_T cut on the $\rho(v_n^2, [p_T])$ correlator. Fig. 4 compares the extracted values for $\text{Var}(v_n^2)_{dyn}$ (a), c_k (b), $\text{cov}(v_n^2, [p_T])$ (c) and $\rho(v_n^2, [p_T])$ (d) computed for the selections $0.2 < p_T < 2.0$ GeV/c and $0.5 < p_T < 2.0$ GeV/c in

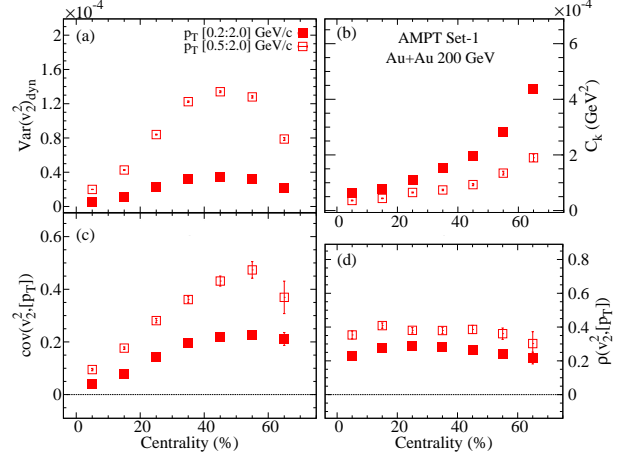


FIG. 4. Comparison of the centrality-dependent values for $\text{Var}(v_n^2)_{dyn}$ (a), c_k (b), $\text{cov}(v_n^2, [p_T])$ (c) and $\rho(v_n^2, [p_T])$ (d) computed for the selections $0.2 < p_T < 2.0$ GeV/c and $0.5 < p_T < 2.0$ GeV/c for Au+Au collisions at 200 GeV with the AMPT model.

Au+Au collisions ($\sqrt{s_{NN}} = 200$ GeV) with the AMPT model. Figs. 4 (a), (c) and (d) indicate a sizable increase in the centrality-dependent values for $\text{Var}(v_n^2)_{dyn}$, $\text{cov}(v_n^2, [p_T])$ and $\rho(v_n^2, [p_T])$ with $\langle p_T \rangle$ [59]. Contrastingly, the centrality-dependent values for c_k indicate a decrease with $\langle p_T \rangle$. The observation of similar experimental patterns could serve as a quantitative constraint to discern between models.

The sensitivity of the $\rho(v_n^2, [p_T])$ correlator to the shape and size of the collision system was investigated using the Event Shape Engineering (ESE) technique [62]. This technique leverages the observation that selections on the magnitude of the event-by-event fluctuations of the v_n coefficients, for a fixed centrality, serve to influence the shape of the collision system [63].

The event-shape selections were performed via a fractional cut on the distribution of the magnitude of the reduced second-order flow vector, q_2 , [62, 64];

$$Q_{2,x} = \sum_i \cos(2\varphi_i), Q_{2,y} = \sum_i \sin(2\varphi_i), \quad (14)$$

$$q_2 = \frac{|Q_2|}{\sqrt{M}}, \quad |Q_2| = \sqrt{Q_{2,x}^2 + Q_{2,y}^2} \quad (15)$$

where Q_2 is the magnitude of the second-order harmonic flow vector calculated within the sub-event $1.5 < \eta < 2.5$, and M is the charged hadron multiplicity for this sub-event. The sub-event $|\eta| < 1.0$ was used to evaluate $\rho(v_n^2, [p_T])$ to ensure the separation between the sub-event used to evaluate q_2 and $\rho(v_n^2, [p_T])$. Note that there are two caveats to the ESE method. First, the q_2 selective power depends on the magnitude of v_2 and the event multiplicity, so the benefit of the technique is handicapped by weak flow values and small event multiplicities [65]. Second, the non-flow effects, such as resonance decays,

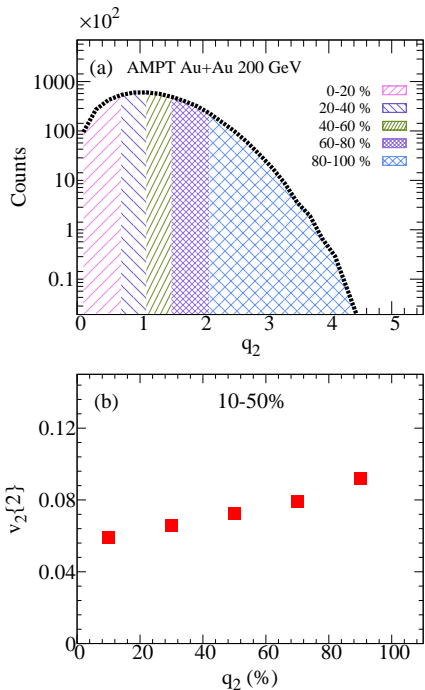


FIG. 5. The q_2 distribution (a) for 10–50% central Au+Au collisions at $\sqrt{s_{NN}} = 200$ GeV, obtained with the sub-event cut $1.5 < \eta < 2.5$ with the AMPT model; $v_2\{2\}$ vs. $q_2(\%)$ (b) for the q_2 selections indicated in panel (a).

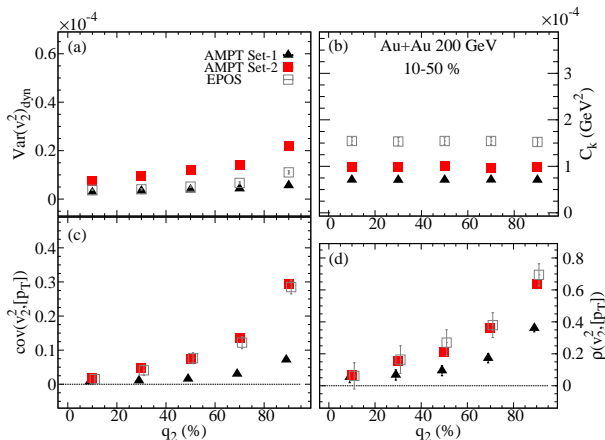


FIG. 6. Comparison of the q_2 -dependent of $\text{Var}(v_n^2)_{dyn}$ (a), c_k (b), $\text{cov}(v_n^2, [p_T])$ (c) and $\rho(v_n^2, [p_T])$ (d) computed for 10–50% central Au+Au collisions ($\sqrt{s_{NN}} = 200$ GeV) obtained with the AMPT and EPOS models.

jets, etc. [66], could bias the q_2 selections. The latter can be minimized via a $\Delta\eta$ separation between the sub-events used for the q_2 selections and $\rho(v_n^2, [p_T])$ evalua-

tions. Fig. 5 (a) shows a representative q_2 distribution for 10-50% central Au+Au collisions at 200 GeV. The $v_2\{2\}$ values which result from the $q_2\%$ selections indicated in panel (a), are shown in Fig. 5 (b). They indicate an essentially linear increase of $v_2\{2\}$ with $q_2\%$.

Figure 6 compare the $q_2\%$ dependence of the values for $\text{Var}(v_2^2)$ (a), c_k (b), $\text{cov}(v_2^2, [p_T])$ (c) and $\rho(v_2^2, [p_T])$ (d), computed for tracks with $0.2 < p_T < 2.0$ GeV/c in Au+Au collisions simulated with the AMPT and EPOS models. A striking feature of these results is the $q_2\%$ -independence of c_k and the essentially quadratic dependence of $\text{cov}(v_2^2, [p_T])$ and $\rho(v_2^2, [p_T])$ on $q_2\%$. These dependencies suggests that data-model comparisons of the $\rho(v_2^2, [p_T])$ correlators extracted in shape-engineered events, could serve as a sensitive constraint for the initial-state eccentricity, and give important insight on the deformation of colliding systems.

IV. SUMMARY

In summary, we have presented extensive model studies to evaluate the model dependence, as well as the response and sensitivity of the $\rho(v_2^2, [p_T])$ correlator to collision-system size and shape and the viscosity of the matter produced in the collisions. We find that the $\rho(v_2^2, [p_T])$ correlators, derived from AMPT and EPOS events which show good agreement between the experimental and theoretical values for $v_2\{2\}$, $v_2\{4\}$ and the ratio $v_2\{4\}/v_2\{2\}$, show good qualitative agreement between the models. Detailed tests with the models further indicate that $\rho(v_2^2, [p_T])$ is sensitive to the initial-state geometry of the collision system, but insensitive to sizable changes in the viscosity of the medium produced in the collisions. These findings strongly suggest that precise differential measurements of $\rho(v_2^2, [p_T])$ as a function of system-size, shape, deformation and beam-energy could provide more stringent constraints to discern between initial-state models and hence, more reliable extractions of η/s .

ACKNOWLEDGMENTS

The authors thank Marysia Stefaniak, Emily Racow, Benjamin Schweid, and Giuliano Giacalone for useful discussions. This research is supported by the US Department of Energy, Office of Nuclear Physics (DOE NP), under contracts DE-FG02-94ER40865 (NM) and DE-FG02-87ER40331.A008 (RL).

[1] E. V. Shuryak, Sov. J. Nucl. Phys. **28**, 408 (1978).
 [2] E. V. Shuryak, Phys. Rept. **61**, 71 (1980).
 [3] B. Muller, J. Schukraft, and B. Wyslouch, Ann. Rev. Nucl. Part. Sci. **62**, 361 (2012), arXiv:1202.3233 [hep-ex].

[4] E. Shuryak, Prog. Part. Nucl. Phys. **53**, 273 (2004), arXiv:hep-ph/0312227.
 [5] P. Romatschke and U. Romatschke, Phys.Rev.Lett. **99**, 172301 (2007), arXiv:0706.1522 [nucl-th].

- [6] M. Luzum and P. Romatschke, Phys.Rev. **C78**, 034915 (2008), arXiv:0804.4015 [nucl-th].
- [7] P. Bozek, Phys. Rev. C **81**, 034909 (2010), arXiv:0911.2397 [nucl-th].
- [8] P. Danielewicz, R. A. Lacey, P. Gossiaux, C. Pinkenburg, P. Chung, J. Alexander, and R. McGrath, Phys. Rev. Lett. **81**, 2438 (1998), arXiv:nucl-th/9803047.
- [9] K. Ackermann *et al.* (STAR), Phys. Rev. Lett. **86**, 402 (2001), arXiv:nucl-ex/0009011.
- [10] K. Adcox *et al.* (PHENIX), Phys. Rev. Lett. **89**, 212301 (2002), arXiv:nucl-ex/0204005 [nucl-ex].
- [11] U. W. Heinz and P. F. Kolb, *Statistical QCD. Proceedings, International Symposium, Bielefeld, Germany, August 26-30, 2001*, Nucl. Phys. **A702**, 269 (2002), arXiv:hep-ph/0111075 [hep-ph].
- [12] T. Hirano, U. W. Heinz, D. Kharzeev, R. Lacey, and Y. Nara, Phys.Lett. **B636**, 299 (2006), arXiv:nucl-th/0511046 [nucl-th].
- [13] P. Huovinen, P. F. Kolb, U. W. Heinz, P. V. Ruuskanen, and S. A. Voloshin, Phys. Lett. **B503**, 58 (2001).
- [14] T. Hirano and K. Tsuda, Phys. Rev. **C66**, 054905 (2002), arXiv:nucl-th/0205043.
- [15] M. Luzum, J. Phys. **G38**, 124026 (2011), arXiv:1107.0592 [nucl-th].
- [16] H. Song, S. A. Bass, U. Heinz, T. Hirano, and C. Shen, Phys. Rev. Lett. **106**, 192301 (2011), [Erratum: Phys. Rev. Lett.109,139904(2012)], arXiv:1011.2783 [nucl-th].
- [17] J. Qian, U. W. Heinz, and J. Liu, Phys. Rev. **C93**, 064901 (2016), arXiv:1602.02813 [nucl-th].
- [18] B. Schenke, S. Jeon, and C. Gale, Phys.Lett. **B702**, 59 (2011), arXiv:1102.0575 [hep-ph].
- [19] D. Teaney and L. Yan, Phys. Rev. **C86**, 044908 (2012), arXiv:1206.1905 [nucl-th].
- [20] F. G. Gardim, F. Grassi, M. Luzum, and J.-Y. Ollitrault, Phys.Rev.Lett. **109**, 202302 (2012), arXiv:1203.2882 [nucl-th].
- [21] R. A. Lacey, D. Reynolds, A. Taranenko, N. N. Ajitanand, J. M. Alexander, F.-H. Liu, Y. Gu, and A. Mwai, J. Phys. **G43**, 10LT01 (2016), arXiv:1311.1728 [nucl-ex].
- [22] N. Magdy, X. Sun, Z. Ye, O. Evdokimov, and R. Lacey, Universe **6**, 146 (2020), arXiv:2009.02734 [nucl-ex].
- [23] C. Shen, U. Heinz, P. Huovinen, and H. Song, Phys. Rev. C **84**, 044903 (2011), arXiv:1105.3226 [nucl-th].
- [24] G. Giacalone, B. Schenke, and C. Shen, Phys. Rev. Lett. **125**, 192301 (2020), arXiv:2006.15721 [nucl-th].
- [25] P. Bozek, Phys. Rev. C **93**, 044908 (2016), arXiv:1601.04513 [nucl-th].
- [26] P. Bozek and H. Mehrabpour, Phys. Rev. C **101**, 064902 (2020), arXiv:2002.08832 [nucl-th].
- [27] B. Schenke, C. Shen, and D. Teaney, Phys. Rev. C **102**, 034905 (2020), arXiv:2004.00690 [nucl-th].
- [28] G. Giacalone, F. G. Gardim, J. Noronha-Hostler, and J.-Y. Ollitrault, Phys. Rev. C **103**, 024909 (2021), arXiv:2004.01765 [nucl-th].
- [29] S. H. Lim and J. L. Nagle, (2021), arXiv:2103.01348 [nucl-th].
- [30] (2021).
- [31] P. Bozek and W. Broniowski, Phys. Rev. C **85**, 044910 (2012), arXiv:1203.1810 [nucl-th].
- [32] G. Giacalone, Phys. Rev. Lett. **124**, 202301 (2020), arXiv:1910.04673 [nucl-th].
- [33] G. Giacalone, Phys. Rev. C **102**, 024901 (2020), arXiv:2004.14463 [nucl-th].
- [34] Z.-W. Lin, C. M. Ko, B.-A. Li, B. Zhang, and S. Pal, Phys. Rev. **C72**, 064901 (2005), arXiv:nucl-th/0411110 [nucl-th].
- [35] H. J. Drescher, M. Hladik, S. Ostapchenko, T. Pierog, and K. Werner, Phys. Rept. **350**, 93 (2001), arXiv:hep-ph/0007198.
- [36] K. Werner, I. Karpenko, T. Pierog, M. Bleicher, and K. Mikhailov, Phys. Rev. C **82**, 044904 (2010), arXiv:1004.0805 [nucl-th].
- [37] K. Werner, B. Guiot, I. Karpenko, and T. Pierog, Phys. Rev. C **89**, 064903 (2014), arXiv:1312.1233 [nucl-th].
- [38] G.-L. Ma and Z.-W. Lin, Phys. Rev. **C93**, 054911 (2016), arXiv:1601.08160 [nucl-th].
- [39] M. R. Haque, M. Nasim, and B. Mohanty, J. Phys. G **46**, 085104 (2019).
- [40] P. P. Bhaduri and S. Chattopadhyay, Phys. Rev. C **81**, 034906 (2010), arXiv:1002.4100 [hep-ph].
- [41] M. Nasim, L. Kumar, P. K. Netrakanti, and B. Mohanty, Phys. Rev. C **82**, 054908 (2010), arXiv:1010.5196 [nucl-ex].
- [42] J. Xu and C. M. Ko, Phys. Rev. C **83**, 021903 (2011), arXiv:1011.3750 [nucl-th].
- [43] N. Magdy, O. Evdokimov, and R. A. Lacey, J. Phys. G **48**, 025101 (2020), arXiv:2002.04583 [nucl-ex].
- [44] Y. Guo, S. Shi, S. Feng, and J. Liao, Phys. Lett. B **798**, 134929 (2019), arXiv:1905.12613 [nucl-th].
- [45] B. Zhang, Comput. Phys. Commun. **109**, 193 (1998), arXiv:nucl-th/9709009 [nucl-th].
- [46] X.-N. Wang and M. Gyulassy, Phys. Rev. **D44**, 3501 (1991).
- [47] M. Gyulassy and X.-N. Wang, Comput. Phys. Commun. **83**, 307 (1994), arXiv:nucl-th/9502021 [nucl-th].
- [48] B.-A. Li and C. M. Ko, Phys. Rev. **C52**, 2037 (1995), arXiv:nucl-th/9505016 [nucl-th].
- [49] J. Xu and C. M. Ko, Phys. Rev. C **83**, 034904 (2011), arXiv:1101.2231 [nucl-th].
- [50] C. R. Allton, S. Ejiri, S. J. Hands, O. Kaczmarek, F. Karsch, E. Laermann, C. Schmidt, and L. Scorzato, Phys. Rev. D **66**, 074507 (2002), arXiv:hep-lat/0204010.
- [51] M. Bleicher *et al.*, J. Phys. G **25**, 1859 (1999), arXiv:hep-ph/9909407.
- [52] S. A. Bass *et al.*, Prog. Part. Nucl. Phys. **41**, 255 (1998), arXiv:nucl-th/9803035.
- [53] H. Petersen, J. Steinheimer, G. Burau, M. Bleicher, and H. Stöcker, Phys. Rev. C **78**, 044901 (2008), arXiv:0806.1695 [nucl-th].
- [54] J. Jia and S. Mohapatra, Phys. Rev. C **88**, 014907 (2013),

- arXiv:1304.1471 [nucl-ex].
- [55] J. Jia, M. Zhou, and A. Trzupek, Phys. Rev. **C96**, 034906 (2017), arXiv:1701.03830 [nucl-th].
- [56] P. Huo, K. Gajdošová, J. Jia, and Y. Zhou, Phys. Lett. B **777**, 201 (2018), arXiv:1710.07567 [nucl-ex].
- [57] C. Zhang, J. Jia, and J. Xu, Phys. Lett. B **792**, 138 (2019), arXiv:1812.03536 [nucl-th].
- [58] B. B. Abelev *et al.* (ALICE), Eur. Phys. J. C **74**, 3077 (2014), arXiv:1407.5530 [nucl-ex].
- [59] G. Aad *et al.* (ATLAS), Eur. Phys. J. C **79**, 985 (2019), arXiv:1907.05176 [nucl-ex].
- [60] C. Zhang, A. Behera, S. Bhatta, and J. Jia, (2021), arXiv:2102.05200 [nucl-th].
- [61] J. Adams *et al.* (STAR), Phys. Rev. C **72**, 014904 (2005), arXiv:nucl-ex/0409033.
- [62] C. Adler *et al.* (STAR), Phys. Rev. **C66**, 034904 (2002), arXiv:nucl-ex/0206001 [nucl-ex].
- [63] B. Abelev *et al.* (ALICE), Phys. Lett. B **719**, 18 (2013), arXiv:1205.5761 [nucl-ex].
- [64] J. Schukraft, A. Timmins, and S. A. Voloshin, Phys. Lett. B **719**, 394 (2013), arXiv:1208.4563 [nucl-ex].
- [65] A. Bzdak, S. Esumi, V. Koch, J. Liao, M. Stephanov, and N. Xu, (2019), arXiv:1906.00936 [nucl-th].
- [66] S. A. Voloshin, A. M. Poskanzer, and R. Snellings, (2008), arXiv:0809.2949 [nucl-ex].